Inorg. Chem. **2005**, *44*, 8884–8898

Barriers to Racemization in C_3-Symmetric Complexes Containing the Hydrotris(2-mercapto-1-ethylimidazolyl)borate (Tm^{Et}) Ligand

Philip J. Bailey,* Alice Dawson, Chiara McCormack, Stephen A. Moggach, Iain D. H. Oswald, Simon Parsons, David W. H. Rankin, and Andrew Turner

School of Chemistry, University of Edinburgh, The King's Buildings, West Mains Road, Edinburgh EH9 3JJ, U.K.

Received April 7, 2005

The tripodal ligands hydrotris(*N*-ethyl-2-mercaptoimidazol-1-yl)borate ($NaTm^{Et}$) (**1**) and hydrotris(*N*-benzyl-2-mercaptoimidazol-1-yl)borate ($NaTm^{Bn}$) (**2**), analogues of the hydrotris(*N*-methyl-2-mercaptoimidazol-1-yl)borate ligand (Tm) containing alternative nitrogen substituents, have been employed to examine the racemization of their C_3-symmetric complexes with both four- and six-coordinate metals. The ligands react at room temperature with metal halides to provide C_3-symmetric metal complexes. The syntheses of the four-coordinate complexes [$Tm^{Et}ZnCl$] (**3**), [$Tm^{Et}CdBr$] (**4**), [$Tm^{Et}HgCl$] (**5**), [$Tm^{Et}CuPPh_3$] (**6**), [$Tm^{Et}AgPPh_3$] (**7**), and [$Tm^{Bn}ZnCl$] (**8**) are reported. The six-coordinate complexes [$Tm^{Et}Ru(p\text{-cymene})$]Cl (**9**), [$Tm^{Et}Ru(p\text{-cymene})$]$PF_6$ (**10**), and [$Tm^{Et}Mn(CO)_3$] (**11**) were also synthesized. The X-ray crystal structures of **3**, **4**, **6**, and **9** are reported. The diastereotopic nature of the ethyl and benzyl hydrogen atoms in the ligands allows the enantiomeric forms of these complexes to be distinguished by ^1H NMR spectroscopy. Variable-temperature (VT) ^1H NMR spectra have thus been used to investigate the energies of the racemization processes occurring in these chiral complexes. In solvents the activation energies to racemization for the four-coordinate complexes lay in the range of 53–77 kJ mol^{-1}. In non-donor solvents the energies are reduced and a dissociative mechanism is therefore implicated. No interconversion could be observed by VT NMR for the six-coordinate complexes in any solvent. To further explore the racemization mechanisms ab initio density functional theory calculations have been conducted on the ground- and transition-state structures of representative six-coordinate [Mn(I)] and four-coordinate [Zn(II)] complexes following a proposed nondissociative mechanism of racemization. The calculated energy barriers to racemization are 163 and 121 kJ mol^{-1}, respectively. It is concluded that the low-energy racemization of substitution-labile four-coordinate complexes occurs via a dissociative mechanism, while substitution-inert six-coordinate complexes experience a significantly higher barrier to racemization. Whether this is due to the operation of a dissociative mechanism with a higher activation barrier or to a nondissociative mechanism remains unknown.

Introduction

Hydrotris(*N*-methyl-2-mercaptoimidazol-1-yl)borate (Tm, Figure 1a) was first reported by Reglinski and Spicer in 1996[1] as a tripodal ligand somewhat analogous to the well-established hydrotris(pyrazolyl)borate (Tp, Figure 1b), but with softer donor atoms. They and others have reported a wide variety of complexes with both transition and main group metals.[2,3] There is, however, a fundamental structural difference between the Tp and Tm ligands in that the number of atoms linking the boron and donor atoms in each arm of

* E-mail: Philip.Bailey@ed.ac.uk.

(1) (a) Garner, M.; Reglinski, J.; Cassidy, I.; Spicer, M. D.; Kennedy, A. R. *J. Chem. Soc., Chem. Commun.* **1996**, 1975−1976. (b) Reglinski, J.; Garner, M.; Cassidy, I. D.; Slavin, P. A.; Spicer, M. D.; Armstrong, D. R. *J. Chem. Soc., Dalton Trans.* **1999**, 2119.

(2) (a) Dodds, C. A.; Kennedy, A. R.; Reglinski, J.; Spicer, M. D. *Inorg. Chem.* **2004**, *43*, 394. (b) Effendy; Gioia Lobbia, G.; Pettinari, C.; Santini, C.; Skelton, B. W.; White, A. H. *Inorg. Chim. Acta* **2000**, *308*, 65. (c) Garcia, R.; Paulo, A.; Domingos, A.; Santos, I. *J. Organomet. Chem.* **2001**, *632*, 41. (d) Bakbak, S.; Incarvito, C. D.; Rheingold, A. L.; Rabinovich, D. *Inorg. Chem.* **2002**, *41*, 998. (e) Kimblin, C.; Churchill, D. G.; Bridgewater, B. M.; Girard, J. N.; Quarless, D. A.; Parkin, G. *Polyhedron* **2001**, *20*, 1891. (f) Seebacher, J.; Vahrenkamp, H. *J. Mol. Struct.* **2003**, *656*, 177. (g) Foreman, M. R. St-J.; Hill, A. F.; White, A. J. P.; Williams, D. J. *Organometallics* **2003**, *22*, 5593. (h) Bailey, P. J.; Lorono-Gonzales, D. J.; McCormack, C.; Parsons, S.; Price, M. *Inorg. Chim. Acta* **2003**, *354*, 61.

(3) Foreman, M. R. St.-J.; Hill, A. F.; White, A. J. P.; Williams, D. J. *Organometallics* **2003**, *22*, 3831.

10.1021/ic0505293 CCC: $30.25
Published on Web 10/25/2005

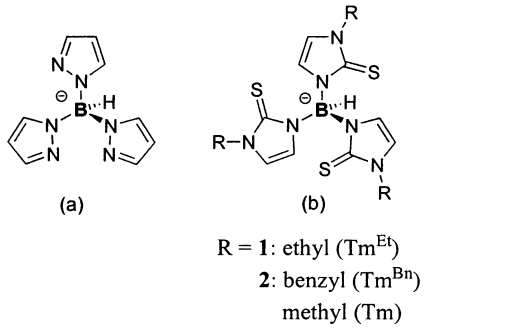

Figure 1. Structures of (a) hydrotris(pyrazolyl)borate (Tp) and (b) hydrotris(*N*-methyl-2-mercaptoimidazol-1-yl)borate (Tm) and substituted derivatives Tm^{Et} and Tm^{Bn}.

the tripod is increased from one (N) in Tp to two (N−C) in the Tm ligand. The consequence of this change in the structures adopted by complexes containing these ligands is striking; while complexation of the Tp ligand provides a bicyclo[2.2.2] cage containing six-membered rings and of ideal C_{3v} symmetry, the Tm ligand forms eight-membered rings with the complexed metal and thus a bicyclo[3.3.3] cage. The angle strain in this type of cage results in torsional twisting of the structure, best visualized as a counter-rotation of the boron and metal centers by 60°, and this reduces the symmetry of the structure to C_3. Complexes of this type thus potentially display a novel form of atropisomerism in which rotation is restricted about a three-dimensional cage structure rather than about a single bond as is normally the case for atropisomers (Figure 2a). Many chiral systems which exhibit atropisomerism have been exploited as ligands in asymmetric catalysis, most notable being the biphenyl derivatives BINAP[4,5] and BINOL.[4,6] Our attention was thus drawn to the Tm ligand by this feature, which is manifest in complexes of both four- and six-coordinate metal centers, and the potential for the exploitation of the chirality thus conferred in the development of a new design for asymmetric catalysts.

The initial step in this project has been to explore the energy barrier to inversion of the cage structure in such complexes and thus the barrier to interconversion between enantiomeric forms of Tm complexes. As has been discussed by Hill, the interconversion between enantiomeric forms may proceed via a dissociative or a nondissociative mechanism (Figure 2b).[3] The former involves the dissociation of one arm of the tripod from the metal followed by Berry pseudorotation of the resulting five-coordinate metal center. Upon recoordination of the dissociated arm a racemic mixture of enantiomers is obtained. The nondissociative process involves conformational interconversion involving a torsional twist of the intact bicyclc cage facilitating racemization between enantiomers via a highly strained C_{3v} symmetric transition state, thus representing an unusual form of atropisomer interconversion. Given the low energy of the pseudorotation process, the activation energy for racemization via the dissociative mechanism would be dependent on the dissociation energy of the metal−donor bond and thus be closely correlated with the lability of the metal center and the trans effect of other ligands present. The operation of this mechanism has been implicated for a series of tungsten complexes [TmW(≡CR)(CO)$_2$] containing a range of alkylidyne substituents (R).[3] The activation energy of the process, as observed by coalescence of inequivalent Tm ligand methyl group signals in the ^{1}H NMR spectra, varied over a considerable range and correlated with the trans effect of the alkylidyne ligands employed. In the case of the nondissociative mechanism it seems likely that the activation energy would depend on the angle strain present in the molecule, and, thus, metal size could be an important factor. To study the energy of the racemization processes in these complexes, we have exploited the Tm^{Et} and Tm^{Bn} ligands (Figure 1b), which contain ethyl and benzyl in place of the *N*-methyl groups found in the Tm ligand. The diastereotopic nature of the methylene hydrogen atoms in these ligands allows the two enantiomeric conformations of the metal−ligand cage to be distinguished by ^{1}H NMR spectroscopy and thus the energy of the racemization process to be measured by line

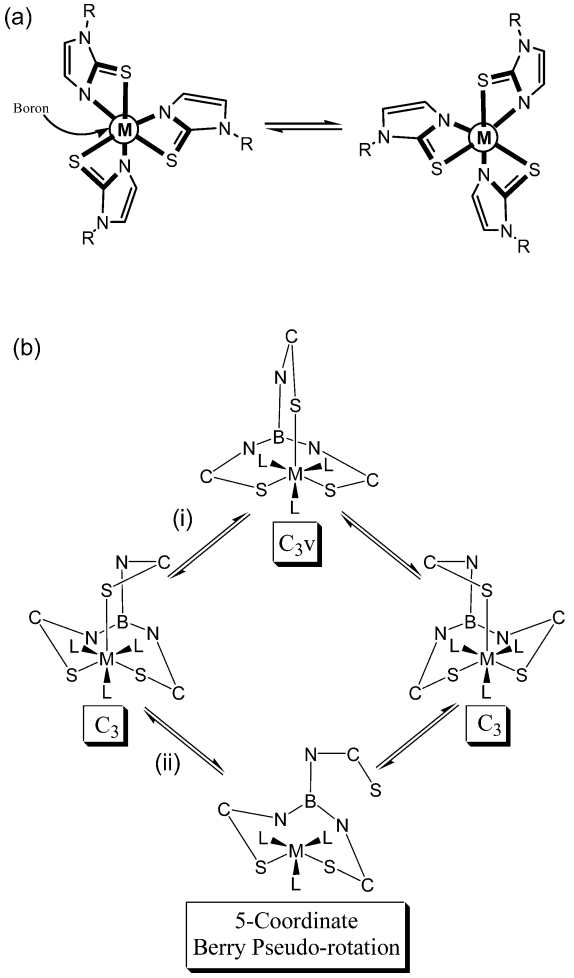

Figure 2. (a) Interconversion (racemization) of chiral atropisomeric metal−Tm complexes viewed along the M−B vector C_3-axis (additional ligands removed for clarity), (b) racemization of a six-coordinate metal−Tm complex [(i) nondissociative; (ii) dissociative] (adapted from ref 3).

(4) Rosini, C.; Franizani, L.; Raffaelli, A.; Salvadori, P. *Synthesis* **1992**, 503;
(5) (a) Noyori, R.; Kitamura, M. *Modern Synthetic Methods*; Springer: Berlin, 1989. (b) Noyori, R.; Ohkuma, T. *Angew. Chem., Int. Ed.* **2001**, *40*, 40.
(6) (a) Pu, L. *Chem. Rev.* **1998**, *98*, 2405. (b) Shibasaki, M.; Sasai, H.; Arai, T. *Angew. Chem., Int. Ed. Engl.* **1997**, *36*, 1237.

shape analysis of variable-temperature NMR spectra of any complex for which the energy lies in a range suitable for this technique.

Experimental Section

General Methods. All reactions were carried out under an atmosphere of dry, oxygen-free dinitrogen, using standard Schlenk techniques. Solvents were freshly distilled over an appropriate drying agent and further degassed before use where necessary. IR spectra were recorded from 4000 to 400 cm^{-1} with a Perkin-Elmer FT-IR instrument. Mass spectra were recorded on a Kratos MS50TC spectrometer. NMR spectra were recorded on a Bruker 250AC spectrometer operating at room temperature. Dymanic NMR experiments were carried out on a Bruker DPX 360. ^1H and ^{13}C chemical shifts are reported in parts per million relative to $SiMe_4$ ($\delta = 0$) and were referenced internally with respect to the protio solvent impurity or the ^{13}C resonances, respectively. Temperatures were measured with the internal NMR probe thermometer and are uncorrected. Multiplicities and peak types are abbreviated: singlet, s; doublet, d; triplet, t; multiplet, m; broad, br; aromatic, ar. $[Ru(p\text{-cymene})_2Cl_2]_2$ [7] and $[Mn(NCMe)_3(CO)_3]PF_6$ [8] were prepared by literature methods. All other chemicals were obtained commercially and used as received. Where satisfactory elemental analyses could not be obtained for new compounds, the full $^{13}C\{^1H\}$ NMR spectrua are provided in the Supporting Information to indicate purity.

2-Mercapto-1-ethylimidazole. This was prepared by adaptation of the method of Kister.[9] To a stirred solution of aminoacetaldehyde diethylacetal (12.0 mL, 82.5 mmol) in tetrahydrofuran (THF, 30 mL) was added ethylisothiocyanate (7.2 mL, 82.2 mmol) slowly to avoid excess heating. The solution was refluxed for 3.5 h. The solvent was stripped in vacuo, and 10% H_2SO_4 (195 mL) was added and the solution refluxed (100 °C) overnight. After adjusting the pH to neutral, the product was extracted into dichloromethane. The solution was dried over magnesium sulfate and the solvent stripped, yielding a brown powder, which was washed repeatedly with hexane. The product was recrystallized from toluene. Yield: 5.89 g, 56%. ^1H NMR ($CDCl_3$): δ 1.23 (t, 3H, $J = 7.2$ Hz, CH_3), 3.89−3.98 (q, 2H, $J = 7.2$ Hz, CH_2), 6.90 (d, 1H, $J = 2.3$ Hz, 4- or 5-H), 7.11(d, 1H, $J = 2.3$ Hz, 4- or 5-H), 12.1 (s, br, N*H*). $^{13}C\{^1H\}$ NMR ($CDCl_3$): δ 14.06 (*C*H_3), 41.58 (*C*H_2), 114.23 (4- or 5-*C*H), 116.87 (4- or 5-*C*H), 158.95 (*C*S). IR (KBr disk): 1282 cm^{-1} (s) ($\nu_{C=S}$). FAB-MS: 128 [M^+].

2-Mercapto-1-benzylimidazole. This was also prepared via Kister's method.[9] To a stirred solution of aminoacetaldehyde diethylacetal (1.10 mL, 7.57 mmol) in THF (5 mL) was added benzylisothiocyanate (1.0 mL, 7.5 mmol) slowly to avoid excess heating. The solution was refluxed under N_2 for 3.5 h. The solvent was stripped in vacuo, and 10% H_2SO_4 (18 mL) was added and the solution refluxed (100 °C) overnight. After adjusting the pH to neutral, the product was extracted into dichloromethane. The solution was dried over magnesium sulfate and the solvent stripped, yielding a brown powder which was washed repeatedly with hexane and dried under vacuum. Yield: 1.19 g, 83%. This compound has previously been synthesized by Matsuda and is described as colorless.[10] The brown color of our product therefore indicates the presence of impurities, although the elemental analysis was satisfactory. The product was used without further purification in the successful synthesis of ligand **2**. ^1H NMR ($CDCl_3$): δ 5.31 (s, 2H, CH_2), 6.65 (d, 1H, $J = 2.6$ Hz, 4- or 5-H), 6.79 (d, 1H, $J = 2.6$ Hz, 4- or 5-H), 7.35−7.45 (m, 5H, ar), 11.71 (s, br, N*H*). $^{13}C\{^1H\}$ NMR ($CDCl_3$): δ 51.64 (*C*H_2), 115.02 (4- or 5-*C*H), 118.91 (4- or 5-*C*H), 128.1, 128.8, 136.2, 143.6 (*C*H, ar), 163.06 (*C*S). FAB-MS: 190 [M^+]. IR (KBr disk): 1278 cm^{-1} (s) ($\nu_{C=S}$). Anal. Found: C, 63.17; H, 5.33; N, 14.41. Calcd for $C_{10}H_{10}N_2S$: C, 63.13; H, 5.33; N, 14.72.

Sodium Hydrotris(*N*-ethyl-2-mercaptoimidazol-1-yl)borate, $NaTm^{Et}$ (1). An adaptation of the literature method[1] for the preparation of NaTm is described. Finely ground $NaBH_4$ (0.44 g, 11.52 mmol) and 2-mercapto-1-ethylimidazole (5.17 g, 40.33 mmol,) were added to a dry round-bottom flask connected to a volumetric device for measurement of H_2 evolution. The stirred mixture was heated slowly to 160 °C and the reaction allowed to proceed until the required volume of gas had been produced. After Soxhlet extraction into chloroform the volume was reduced and the product isolated by filtration. Yield: 2.54 g, 53%. ^1H NMR (dimethyl sulfoxide (DMSO)): δ 1.25 (t, 9H, $J = 9$ Hz, CH_3), 3.97 (q, 6H, $J = 9$ Hz, CH_2), 6.44 (d, 3H, $J = 2$ Hz, 4- or 5-H), 6.88 (d, 3H, $J = 2$ Hz, 4- or 5-H). $^{13}C\{^1H\}$ NMR ($CDCl_3$): δ 15.52 (*C*H_3), 43.16 (*C*H_2), 117.79 (4- or 5- *C*H), 120.20 (4- or 5-*C*H), 161.97 (*C*S). FAB-MS: 416 [M^+]. IR (KBr, cm^{-1}) ν(B−H): 2482. MS (FAB): 416 [M^+], 393 [$M^+ - Na$].

Sodium Hydrotris(*N*-benzyl-2-mercaptoimidazol-1-yl)borate, $NaTm^{Bn}$ (2). An adaptation of the literature method[1] is described. A solution of 2-mercapto-1-benzylimidazole (2.0 g, 10.51 mmol) and $NaBH_4$ (0.133 g, 3.52 mmol) in dry toluene (40 mL) was refluxed for 3 days. The volume of the solution was reduced and the product isolated by filtration. Yield: 1.50 g, 71%. ^1H NMR ($CDCl_3$): δ 5.21 (s, 2H, CH_2), 6.07 (d, 3H, $J = 2$ Hz, 4- or 5-H), 6.50 (d, $J = 2$ Hz, 3H, 4- or 5-H), 7.06−7.28 (m, 15H, ar). $^{13}C\{^1H\}$ NMR ($CDCl_3$): δ 50.48 (*C*H_2), 117.45 (4- or 5- *C*H), 119.20 (4- or 5- *C*H), 127.64 (*p*-*C*H), 128.01 (*o*-*C*H), 128.64 (*m*-*C*H), 136.44 (C_{quat}), 162.17 (*C*S). IR (KBr): 2478 cm^{-1} (s) (ν_{B-H}). MS(FAB): 603 [M^+].

[Tm^{Et}ZnCl] (3). To a stirred suspension of $ZnCl_2$ (34 mg, 0.249 mmol) in CH_2Cl_2 (10 mL) was added $NaTm^{Et}$ (105 mg, 0.252 mmol) in one portion. After a few minutes, the reactants had dissolved and a white precipitate had formed. The reaction was stirred for 2 h. The solution was filtered and layered with pentane. The crystals that formed were isolated and dried under vacuum. Yield: 75 mg, 61%. ^1H NMR ($CDCl_3$): δ 1.28 (t, 9H, $J = 7$ Hz, CH_3), 3.92−4.19 (m, 6H, CH_2), 6.80 (d, 3H, $J = 2$ Hz, 4- or 5-H), 6.82 (d, 3H, $J = 2$ Hz, 4- or 5-H). $^{13}C\{^1H\}$ NMR ($CDCl_3$): δ 15.93 (*C*H_3), 43.16 (*C*H_2), 119.96 (4- or 5- *C*H), 122.26 (4- or 5-*C*H), 156.77 (*C*S). FAB-MS: 459 [$M^+ - Cl$]. IR (KBr): 2423 cm^{-1} ν(B−H).

[Tm^{Et}CdBr] (4). Compound **4** was prepared similarly to complex **3**, by using $CdBr_2 \cdot 4H_2O$ (83 mg, 0.241 mmol) and $NaTm^{Et}$ (100 mg, 0.240 mmol) in CH_2Cl_2 (5 mL). After 4 h the solution was filtered through Celite and the solvent stripped, yielding a white solid. Yield: 120 mg, 85%. ^1H NMR ($CDCl_3$): δ 1.31 (t, 9H, $J = 5$ Hz, CH_3), 3.94−4.15 (m, 6H, CH_2), 6.74 (d, 3H, $J = 1$ Hz, 4- or 5-H), 6.79 (d, 3H, $J = 1$ Hz, 4- or 5-H). $^{13}C\{^1H\}$ NMR ($Cl_2CDCDCl_2$): δ14.30 (CH_3), 42.44 (CH_2), 116.01(4- or 5-*C*H), 118.62 (4- or 5-*C*H), 153.59 (*C*S). IR (KBr): 2407 cm^{-1} ν(B−H). FAB-MS: 585 [M^+].

[Tm^{Et}HgCl] (5). Compound **5** was prepared similarly to complex **3**, by using $HgCl_2$ (55 mg, 0.201 mmol) and $NaTm^{Et}$ (84 mg, 0.202

(7) Bennet, M. A.; Smith, A. K. *J. Chem. Soc., Dalton Trans.* **1974**, 233.
(8) (a) Reimann, R. H.; Singleton, E. *J. Organomet. Chem.* **1973**, *54*, C24. (b) Reimann, R. H.; Singleton, E. *J. Chem. Soc., Dalton Trans.* **1974**, 808.
(9) Kister, J.; Assef, G.; Mille, G.; Metzger, J. *Can. J. Chem.* **1979**, *57*, 813.
(10) Matsuda, K.; Yanagisawa, I.; Isomura, Y.; Mase, T.; Shibanuma, T. *Synth. Commun.* **1997**, *27*, 3565.

mmol) in CH_2Cl_2 (10 mL). After 2 h the solution was filtered and the solvent stripped, yielding a pale yellow solid. Yield: 124 mg, 98%. ^{1}H NMR ($CDCl_3$): δ 1.27 (t, 9H, J = 6 Hz, CH_3), 4.04 (m, br, 6H, CH_2), 6.72 (s, br, 3H, 4- or 5-H), 6.90 (s, br, 3H, 4- or 5-H). ^{13}C{^{1}H} NMR ($CDCl_3$): δ 14.77 (*C*H$_3$), 42.66 (*C*H$_2$), 118.19 (4- or 5- *C*H), 123.91 (4- or 5-*C*H), 155.30 (*C*S). IR (KBr): 2430 cm^{-1} ν(B−H). FAB-MS: 621 [M$^+$].

[Tm^{Et}Cu(PPh$_3$)] (6). To a stirred solution of CuCl (12 mg, 0.12 mmol) and PPh_3 (63 mg, 0.24 mmol) in methanol (5 mL) was added NaTm^{Et} (50 mg, 0.12 mmol) in one portion. The reaction was stirred for 2.5 h and the white precipitate filtered off, washed with ether, and dried in vacuo. Yield: 61 mg, 70%. ^{1}H NMR ($CDCl_3$): δ 1.27 (t, 9H, J = 7 Hz, CH_3), 4.06−4.14 (m, br, 6H, CH_2), 6.74 (d, 3H, J = 2 Hz, 4- or 5-H), 6.87 (s, br, 3H, 4- or 5-H). ^{13}C{^{1}H} NMR ($CDCl_3$): δ 15.71 (*C*H$_3$), 42.95 (*C*H$_2$), 117.32 (4- or 5-*C*H), 123.54 (s, C$_p$), 129.19 (d, J(^{13}C−^{31}P) = 9 Hz, C$_m$), 130.10 (4- or 5-*C*H), 133.05 (d, J(^{13}C−^{31}P) = 18 Hz, C$_i$), 135.11 (d, J(^{13}C−^{31}P) = 15.4 Hz, C$_m$), 162.10 (*C*S). IR (KBr): 2375 cm^{-1} ν(B−H). FAB-MS: 719 [M$^+$].

[Tm^{Et}Ag(PPh$_3$)] (7). To a stirred solution of $AgBF_4$ (50 mg, 0.257 mmol) and PPh_3 (67 mg, 0.556 mmol) in THF (10 mL) was added NaTm^{Et} (107 mg, 0.257 mmol) in one portion. After the addition a white precipitate formed and the reaction was stirred at room temperature for 2 h. The solvent was stripped, and the product taken into CH_2Cl_2 and filtered and the solvent removed under vacuum. Yield: 151 mg, 77%. ^{1}H NMR ($CDCl_3$): δ 1.13 (t, 9H, J = 9 Hz, CH_3), 3.65−3.71 (m, br, 6H, CH_2), 6.65 (d, 3H, J = 2 Hz, 4- or 5-H), 6.74 (d, 3H, J = 2 Hz, 4- or 5-H), 7.19−7.77 (m, 15H, ar). ^{13}C{^{1}H} NMR ($CDCl_3$): δ 14.32 (*C*H$_3$), 42.08 (*C*H$_2$), 116.74 (4- or 5-*C*H), 128.44 (d, J(^{13}C−^{31}P) = 8 Hz, C$_m$), 129.17 (4- or 5-*C*H), 131.97 (d, J(^{13}C−^{31}P) = 10 Hz, C$_o$), 133.73 (d, J(^{13}C−^{31}P) = 18 Hz, C$_i$), 134.93 (s, C$_p$), 161.50 (*C*S). IR (KBr): 2383 cm^{-1} ν(B−H); FAB-MS: 764 [M$^+$].

[ZnTm^{Bn}Cl] (8). $ZnCl_2$ (102 mg, 0.748 mmol) and NaTm^{Bn} (451 mg, 0.748 mmol) were stirred together in dichloromethane (30 mL) at room temperature for 4 h. The resulting solution was filtered through Celite and the solvent stripped, yielding a white solid. Yield: 396 mg, 78%. ^{1}H NMR ($CDCl_3$): δ 5.06−5.39 (q, 6H, CH_2), 6.69 (d, 3H, 4- or 5-C*H*), 6.81 (d, 3H, 4- or 5-C*H*), 7.19−7.32 (m, 15H, ar). ^{13}C{^{1}H}NMR ($CDCl_3$): 51.02 (*C*H$_2$), 118.95 (4- or 5-*C*H), 124.31 (4- or 5-*C*H), 128.28, 128.47, 128.90 (*C*H, ar), 135.19 (*C*$_{quat}$), 157.00 (*C*S). FAB-MS: 645 [M$^+$ − Cl]. IR (KBr): 2435 cm^{-1} ν_{B-H}.

[Tm^{Et}Ru(p-cymene)]Cl (9). To a stirred and heating solution of [Ru(*p*-cymene)Cl$_2$]$_2$ (37 mg, 0.060 mmol) in ethanol (5 mL) was added a solution of NaTm^{Et} (50 mg, 0.120 mmol) in ethanol (5 mL). The orange solution immediately turned reddish brown, and the solution was refluxed for 1 $^1/_2$ h. The solvent was removed in vacuo and the product dissolved in dichloromethane and filtered and the solvent stripped, yielding an orange powder. Yield: 65 mg, 81%. ^{1}H NMR ($CDCl_3$): δ 1.15 (d, 6H, J = 7 Hz, CH_3), 1.34 (t, 9H, J = 7 Hz, CH_3), 2.17 (s, 3H, CH_3), 2.90 (sept, 1H, J = 7 Hz, C*H*), 4.05−4.20 (m, 6H, CH_2), 5.24 (d, 1H, J = 6 Hz, ar CH), 5.29 (d, 1H, J = 6 Hz, ar CH), 5.36 (d, 1H, J = 6 Hz, ar CH), 5.39 (d, 1H, J = 6 Hz, ar CH), 6.81 (d, 3H, J = 2 Hz, 4- or 5-H), 7.02 (d, 3H, J = 2 Hz, 4- or 5-H). ^{13}C{^{1}H} NMR ($CDCl_3$): δ 15.35 (Et *C*H$_3$), 18.31 (*C*H$_3$), 22.17 (^{i}Pr *C*H$_3$), 22.75 (^{i}Pr *C*H$_3$), 30.12 (^{i}Pr *C*H), 42.65 (Et *C*H$_2$), 83.85 (ar *C*H), 84.58 (ar *C*H), 85.64 (ar *C*H), 86.09 (ar *C*H), 101.15 (ar C$_{quat}$), 106.57 (ar C$_{quat}$), 119.18 (4- or 5-*C*H), 124.58 (4- or 5- *C*H), 154.85 (*C*S). FAB-MS: 629 [M$^+$]. IR (KBr): 2428 cm^{-1} ν(B−H).

[Tm^{Et}Ru(p-cymene)]PF$_6$ (10). To a stirred suspension of [Tm^{Et}Ru(p-cymene)]Cl (75 mg, 0.13 mmol) in THF (10 mL) was added NH_4PF_6 (25 mg, 0.015 mmol) in one portion. After the addition a white precipitate formed and the reaction was stirred at room temperature for 1 h. The mixture was filtered through Celite and the solvent stripped, yielding a purple solid. Yield: 87 mg, 87%. ^{1}H NMR ($CDCl_3$): δ 1.17 (d, 6H, J = 7 Hz, CH_3), 1.25 (t, 9H, J = 7 Hz, CH_3), 2.15 (s, 3H, CH_3), 2.90 (sept, 1H, J = 7 Hz, C*H*), 4.02−4.18 (m, 6H, CH_2), 5.12 (d, 1H, J = 6 Hz, ar CH), 5.16 (d, 1H, J = 6 Hz, ar CH), 5.27 (d, 1H, J = 6 Hz, ar CH), 5.29 (d, 1H, J = 6 Hz, ar CH), 6.80 (d, 3H, J = 2 Hz, 4- or 5-H), 6.89 (d, 3H, J = 2 Hz, 4- or 5-H). ^{13}C{^{1}H} NMR ($CDCl_3$): δ 16.43 (Et *C*H$_3$), 19.39 (*C*H$_3$), 23.31 (^{i}Pr *C*H$_3$), 23.85 (^{i}Pr *C*H$_3$), 31.30 (^{i}Pr *C*H), 43.82 (Et *C*H$_2$), 84.95 (ar *C*H), 85.68 (ar *C*H), 86.80 (ar *C*H), 87.31 (ar *C*H), 102.41 (ar C$_{quat}$), 107.75 (ar C$_{quat}$), 120.03 (4- or 5-*C*H), 125.66 (4- or 5-*C*H), 156.28 (*C*S). FAB-MS: 629 [M$^+$].

[Tm^{Et}Mn(CO)$_3$] (11). To a stirred suspension of [Mn(NCMe)$_3$(CO)$_3$]PF$_6$ (150 mg, 0.368 mmol) in ethanol (10 mL) was added NaTm^{Et} (153 mg, 0.367 mmol) in one portion. A yellow precipitate formed almost immediately, and the reaction was stirred for 1 h. The solid was filtered off, washed with a small amount of ethanol, and died under vacuum. Yield: 156 mg, 80%. ^{1}H NMR ($Cl_2CDCDCl_2$): δ 1.34 (t, 9H, J = 8 Hz, CH_3), 4.01−4.31 (m, 6H, CH_2), 6.81 (d, 3H, J = 2 Hz, 4- or 5-H), 6.85 (d, 3H, J = 2 Hz, 4- or 5-H). FAB-MS: 532 [M$^+$]. IR ($CHCl_3$): 2007 cm^{-1} (s) , 1908 (s, br) ν_{CO}. IR (KBr disk): 1987(s), 1883 cm^{-1} (s) ν_{CO}. The very poor solubility of this complex even in strongly polar solvents (DMSO, MeCN) meant that a satisfactory ^{13}C NMR spectrum could not be obtained. After extensive drying under vacuum a satisfactory elemental analysis was obtained: Found: C, 40.19; H, 4.44; N, 15.71. Calcd for $C_{18}H_{22}MnBN_6O_3S_3$: C, 40.61; H, 4.17; N, 15.79.

Ab Initio Calculations. Using the Gaussian 98 suite of quantum chemistry programs,[11] we have performed geometry optimizations on the ground-state and the transition-state structures of six-coordinate [Mn(II)] and four-coordinate [Zn(II)] C_3-symmetric complexes undergoing nondissociative racemization. All calculations included electron correlation using second-order Moller−Plesset perturbation theory (MP2) and used the LANL2DZ basis set. This basis set includes relativistic effects for heavy atoms through effective core potentials [ECPs; S (Ne core), Mn (Ne core), Zn (Ar core)] and uses the 6-31G basis set to describe the valence electrons and light atoms [H, B, C, N, O, S(3s3p), Mn(3s3p4s3d), Zn(4s3d)]. The six-coordinate Mn(II) complex and the four-coordinate Zn(II) complex ground states were both modeled with no symmetry to allow for complete relaxation of the structure. For the transition states, the torsional angles defining the twists of the ligand arms, from the metal atom through the sulfur atoms to the rings, were fixed at 0° and then these constrained geometries were optimized. Crystal structures were used as the starting point for all ground-state geometry optimizations. The optimized ground-state structures were used as the starting points for the transition-state optimizations, apart from the constraints described above.

(11) Frisch, M. J.; Trucks, G. W.; Schlegel, H. B.; Scuseria, G. E.; Robb, M. A.; Cheeseman, J. R.; Zakrzewski, V. G.; Montgomery, J. A., Jr.; Stratmann, R. E.; Burant, J. C.; Dapprich, S.; Millam, J. M.; Daniels, A. D.; Kudin, K. N.; Strain, M. C.; Farkas, O.; Tomasi, J.; Barone, V.; Cossi, M.; Cammi, R.; Mennucci, B.; Pomelli, C.; Adamo, C.; Clifford, S.; Ochterski, J.; Petersson, G. A.; Ayala, P. Y.; Cui, Q.; Morokuma, K.; Malick, D. K.; Rabuck, A. D.; Raghavachari, K.; Foresman, J. B.; Cioslowski, J.; Ortiz, J. V.; Baboul, A. G.; Stefanov, B. B.; Liu, G.; Liashenko, A.; Piskorz, P.; Komaromi, I.; Gomperts, R.; Martin, R. L.; Fox, D. J.; Keith, T.; Al-Laham, M. A.; Peng, C. Y.; Nanayakkara, A.; Gonzalez, C.; Challacombe, M.; Gill, P. M. W.; Johnson, B.; Chen, W.; Wong, M. W.; Andres, J. L.; Gonzalez, C.; Head-Gordon, M.; Replogle, E. S.; Pople, J. A. *Gaussian 98*, Revision A.7; Gaussian, Inc.: Pittsburgh, PA, 1998.

Table 1. Crystallographic Data for [$Tm^{Et}Cu(PPh_3)$] (**6**) and [$Tm^{Et}Ru(p\text{-cymene})$]Cl (**9**)

	6	**9**
cryst descripn	colorless block	red plate
empirical formula	$C_{33}H_{37}BCuN_6PS_3$	$C_{25}H_{38}BClN_6ORuS_3$
M_w	719.23	682.12
T (K)	150(2)	220(2)
cryst syst	trigonal	monoclinic
space group	$R\bar{3}$	$P2_1/n$
a (Å)	15.5870(16)	10.2524(14)
b (Å)	15.5870(16)	12.0839(16)
c (Å)	12.144(2)	24.863(3)
α (deg)	90	90
β (deg)	90	91.353(2)
γ (deg)	120	90
V (Å^3)	2555.1(6)	3079.4(7)
Z	3	4
μ(Mo Kα) (mm^{-1})	0.906	0.829
independent reflecs	1619 [R(int) = 0.036]	7434 [R(int) = 0.0390]
data with $\|F\| > 4\sigma(\|F\|)$]	1606	5968
param refined	138	358
abs correcn	semiempirical from equivalents (T_{min} = 0.630, T_{max} = 0.700)	multiscan (T_{min} = 0.459, T_{max} = 0.720)
R	0.0213	0.0425
R_w	0.0504	0.0959

X-ray Crystallography. Crystallographic data for [$Tm^{Et}Cu(PPh_3)$] (**6**) and [$Tm^{Et}Ru(p\text{-cymene})$]Cl (**9**) are presented in Table 1. Full crystallographic details for [$Tm^{Et}ZnCl$] (**3**) and [$Tm^{Et}CdBr$] (**4**) are provided in the Supporting Information.

All data sets were collected with Mo Kα radiation on a Bruker SMART APEX CCD diffractometer equipped with an Oxford Cryosystems low-temperature device. Absorption corrections were carried out using the multiscan procedure SADABS. The structures **3**, **6**, and **9** were solved by direct methods (SHELXS or SIR92); that of **4** was solved by Patterson methods (DIRDIF). All structures were refined by full-matrix least-squares against F^2 (SHELXL for **3** and **9** and CRYSTALS for **4** and **6**). H-atoms were generally placed in idealized positions and allowed to ride on their parent atoms. In **3** and **9** methyl groups were treated with the Sheldrick rotating rigid group procedure; in **4** and **6** the H-atom attached to B was located in a difference map and its position refined; in **9** the H-atoms attached to the water of crystallization were refined subject to explicit geometry restraints. All non-H atoms were refined with anisotropic displacement parameters.

Results and Discussion

The synthesis of the ligand hydrotris(*N*-ethyl-2-mercaptoimidazol-1-yl)borate as its sodium salt ($NaTm^{Et}$, **1**), was based on the published synthesis of the Tm ligand.[1] Thus, sodium borohydride and 3 equiv of 2-mercapto-1-ethylimidazole reacted in the melt to produce $NaTm^{Et}$ with elimination of dihydrogen. The benzyl-substituted ligand, sodium hydrotris(*N*-benzyl-2-mercaptoimidazol-1-yl)borate (Tm^{Bn}, **2**), was also synthesized by an adaptation of the literature method.[12] The four-coordinate complexes [$Tm^{Et}ZnCl$] (**3**), [$Tm^{Et}CdBr$] (**4**), and [$Tm^{Et}HgCl$] (**5**) were synthesized by reaction of the appropriate metal dihalide with $NaTm^{Et}$ at room temperature in dichloromethane. The group 11 complexes [$Tm^{Et}Cu(PPh_3)$] (**6**) and [$Tm^{Et}Ag(PPh_3)$] (**7**) were produced in a similar manner from CuCl and $AgBF_4$, respectively, with the addition of triphenylphosphine to complete the coordination sphere. The complex [$Tm^{Bn}ZnCl$] (**8**) containing the benzyl-substituted ligand Tm^{Bn} was prepared in a reaction similar to those forming the Tm^{Et} analogues. The six-coordinate complexes [$Tm^{Et}Ru(p\text{-cym})$]Cl (**9**), [$Tm^{Et}Ru(p\text{-cym})$]PF_6 (**10**), and [$Tm^{Et}Mn(CO)_3$] (**11**) were also synthesized via similar routes from metal halide complex precursors.

The complexes **3**, **4**, **6**, and **9** were characterized by X-ray crystallography. Details of the structures of **3** and **4** are provided in the Supporting Information, while those of **6** and **9** are discussed here as representative examples of complexes containing four- and six-coordinate metal centers.

X-ray Structures. The crystal structure of [$CuTm^{Et}PPh_3$] (**6**) is shown in Figure 3 with selected bond lengths and angles listed in Table 2. The complex crystallizes in space group $R\bar{3}$, and the B−Cu vector is located on a crystallographic 3-fold axis making the three donor heterocycles crystallographically equivalent. The copper center adopts a distorted-tetrahedral geometry with S−Cu−S and S−Cu−P bond angles of 102.43(2) and 115.83(2)°, respectively. The

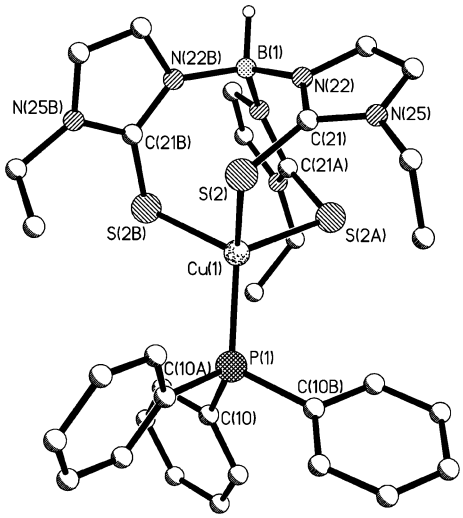

Figure 3. Molecular structure of [$Tm^{Et}Cu(PPh_3)$] (**6**) (hydrogen atoms omitted for clarity).

(12) Bakbak, S.; Bhatia, K.; Incarvito, C. D.; Rheingold, A. L.; Rabinovich, D. *Polyhedron* **2001**, *20*, 3343.

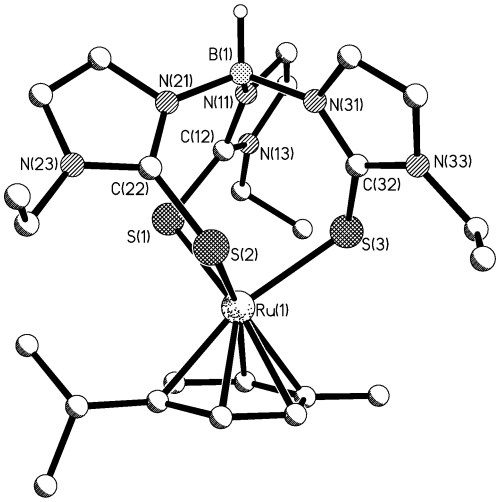

Figure 4. Molecular structure of [Tm^{Et}Ru(*p*-cymene)]Cl·H_2O (**9**) (hydrogen atoms, the Cl^- ion, and H_2O solvent molecule have been omitted for clarity).

Table 2. Selected Bond Lengths (Å) and Angles (deg) for [Tm^{Et}Cu(PPh$_3$)] (**6**) (See Also Table 4)

Cu(1)−S(2)	2.3873(6)	S(2)-Cu(1)-S(2A)	102.43(2)
Cu(1)−P(1)	2.2286(12)	Cu(1)−S(2)−C(21)	97.48(9)
S(2)−C(21)	1.723(2)	S(2)−C(21)−N(22)	127.84(19)
C(21)−N(22)	1.349(3)	N(22)−B(1)−N(22B)	112.30(16)
B(1)−N(22)	1.542(2)	S(2)−Cu(1)−P(1)	115.827(16)

S−Cu−S angles are significantly smaller than found in the previously reported[13] [TmCu(*m*-tolyl$_3$P)] [104.59(6)°] and [TmCu(*p*-tolyl$_3$P)] [107.10(4)°], while the S−Cu−P angles are significantly larger than those in these two complexes [114.00(4) and 111.75(2)°, respectively]. There are also differences in the Cu−S [2.3873(6) Å] and Cu−P [2.2286(12) Å] distances, which are significantly longer than in their *m*-tolyl$_3$P and *p*-tolyl$_3$P analogues [2.357(2)/2.217(3) and 2.3323(9)/2.226(1) Å, respectively]. The variability of the angles around the copper center in these complexes induced by relatively minor changes in the ligand steric properties indicates that minor distortion of the S−M−S angles is a relatively low energy process. In these d^{10} metal ions this energy will be determined by the angle strain in the bicyclic cage and not by any geometric preferences of the metal.

The crystal structure of **9** is shown in Figure 4 with selected bond lengths and angles listed in Table 3. The complex crystallizes with one molecule of water in the unit cell. The ruthenium atom is coordinated by the three sulfur donors with an average Ru−S distance of 2.419 Å. The S−Ru−S angles [90.76(3), 88.97(3), and 93.12(3)°] deviate only slightly from normal octahedral angles and are very similar to those found in [TmRu(*p*-cymene)]Cl [90.40(3), 93.38(3), and 91.31(3)°].[2h] The average Ru−C(*p*-cymene) distance is 2.206 Å, which is similar to the average Ru−C(*p*-cymene) distances in [RuTm(*p*-cymene)]Cl [2.210 Å] and other Ru(*p*-cymene) fragments in complexes such as [RuTp(*p*-cymene)] (2.206 Å)[14] and [(Ru(*p*-cymene){η^2-(^{i}PrN)$_2$PPh(NH^{i}Pr)}]$^+$ (2.185 Å).[15]

(13) Gioia Lobbia, G.; Pettinari, C.; Santini, C.; Somers, N.; Skelton, B. W.; White, A. H. *Inorg. Chim. Acta* **2001**, *319*, 15.
(14) Bhambri, S.; Tocher, D. A. *Polyhedron* **1996**, *15*, 2763.
(15) Bailey, P. J.; Grant, K. J.; Parsons, S. *Organometallics* **1998**, *17*, 551.

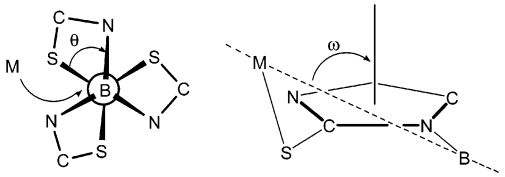

Figure 5. Definitions of θ and ω characterizing the degree of *twist* in metal−Tm complexes (adapted from ref 3).

Table 3. Selected Bond Lengths (Å) and Angles (deg) for [Tm^{Et}Ru(*p*-cymene)]Cl.H_2O (**9**) (See Also Table 4)

Ru(1)−S(1)	2.4206(8)	Ru(1)−S(1)−C(12)	108.41(9)
Ru(1)−S(2)	2.4254(7)	Ru(1)−S(2)−C(22)	108.92(9)
Ru(1)−S(3)	2.4106(8)	Ru(1)−S(3)−C(32)	110.68(10)
S(1)−C(12)	1.729(3)	S(1)−C(12)−N(11)	128.0(2)
S(2)−C(22)	1.730(3)	S(2)−C(22)−N(21)	129.1(2)
S(3)−C(32)	1.727(3)	S(3)−C(32)−N(31)	128.8(2)
C(12)−N(11)	1.341(4)	C(12)−N(11)−B(1)	130.7(2)
N(11)−B(1)	1.547(4)	C(22)−N(21)−B(1)	132.0(2)
C(22)−N(21)	1.347(3)	C(32)−N(31)−B(1)	132.0(2)
N(21)−B(1)	1.544(4)	N(11)−B(1)−N(21)	113.7(2)
C(32)−N(31)	1.355(3)	N(11)−B(1)−N(31)	109.9(2)
N(31)−B(1)	1.547(4)	N(21)−B(1)−N(31)	112.2(2)
		S(1)−Ru(1)−S(2)	92.12(3)
		S(1)−Ru(1)−S(3)	90.76(3)
		S(2)−Ru(1)−S(3)	88.97(3)

An analysis of the torsion angles characterizing the degree of *twist* present in complexes of the Tm ligand has been undertaken by Hill, and he has suggested the adoption of two torsion angles to parametrize this feature of the complexes; N−B−M−S (θ, mean θ^m) and that made by the normal to the imidazole ring and the B−M vector (ω, mean ω^m) (Figure 5).[3] From the data available at this time, θ^m for complexes with four-coordinate metal centers was found to range between 40.2 and 47.5° and ω^m between 52.1 and 59.0°, while for complexes with six-coordinate metals the θ^m range was 46.5−49.4°, and the ω^m range was 55.0−61.7°. Although there is significant overlap between the ranges for four- and six-coordinate systems, it seems that there is a tendency for both parameters to be larger for the six-coordinate metal complexes. However, as discussed above in relation to four-coordinate copper complexes, even closely related complexes can vary significantly in their coordination geometry. For the three complexes [Tm^{Et}Cu(PPh$_3$)] (**6**), [TmCu(*m*-tolyl$_3$P)], and [TmCu(*p*-tolyl$_3$P)] the θ^m values vary over a range of 7° (Table 4), while ω^m values lie in a narrower range of 0.6°. This variability is more starkly illustrated in the structure of [TmMn(CO)$_3$] which we have reported previously.[2h] The ω^m values for the two independent molecules in the unit cell of this complex are not significantly different, both being 60.8°; however, the θ^m values for the two molecules differ by 5.5°. Only crystal packing forces can be responsible for this difference. A similar picture is seen for [TmRe(CO)$_3$], which is isomorphous with its Mn analogue.[2c] The two independent molecules in this structure have θ^m values which differ by 4.4°, while their ω^m values differ by only 0.4°. From these examples it appears that, within the crystal lattice, distortion of ω is a somewhat higher energy process than that of θ. What this implies is that minor relative twisting of the metal and boron centers of the bicyclic cage is a relatively low energy process; in other words, with respect to the torsion between B and M centers, Tm

Table 4. Metrical Parameters for Representative Tm Complexes

	θ^m (deg)	ω^m (deg)	M−S bond distance (Å)	S−M−S bond angle (deg)	C−S−M bond angle (deg)
$[Tm^{Et}Cu(PPh_3)]$ (**6**)[a]	47.2	58.4	2.3868(8)	102.43(2)	97.52(12)
$[TmCu(m\text{-tolyl}_3P)]$[11 a]	45.5	58.7	2.357(2)	104.59(6)	98.5(3)
$[TmCu(p\text{-tolyl}_3P)]$[11 a]	40.2	59.0	2.3323(9)	107.10(4)	103.8(1)
$[TmMn(CO)_3]$[2h a,b]	−41.4	60.8	2.4015(5)	94.329(18)	111.54(6)
	−46.9	60.8	2.4277(5)	92.981(19)	105.42(6)
$[TmRe(CO)_3]$[2c a,b]	42.8	60.3	2.510(2)	91.82(7)	109.77
	47.2	59.9	2.521(2)	90.48(7)	105.49
$[Tm^{Et}Ru(p\text{-cymene})]^+$ (**10**)	−46.1	55.2	2.4206(8)	92.12(3)	108.41(9)
			2.4254(7)	90.76(3)	108.92(9)
			2.4106(8)	88.97(3)	110.68(10)

[a] Crystallographically imposed 3-fold symmetry. [b] Two independent molecules in the unit cell.

complexes sit in a relatively flat-bottomed energy well. However, this is not the full picture as, for these relatively minor distortions, changes in θ are not correlated with those in ω, and the question of how θ can vary so much without affecting ω to any significant extent within a fully connected cage structure remains. Although the metal−sulfur bond distances for these complexes vary slightly (Table 4), this cannot account for these observations since changes in the M−S distance would affect ω as well as θ. This may be appreciated by visualizing the progressive reduction of the M−S distances resulting, in extremis, in the formation of a C_{3v} symmetric structure as the distance becomes zero when $\theta = 0°$ and $\omega = 90°$, a structure analogous to those formed by the Tp ligand. The observed variation between the structures is best considered as a rotation of the metal fragment, while the Tm ligand structure remains static and rigid. The apparent low energy of this distortion illustrates the coordinative flexibility of the sulfur donors and is manifest in the variation in the C−S−M bond angles between related complexes (Table 4). What is immediately obvious is that these angles at sulfur are significantly larger in the six-coordinate complexes than in the four-coordinate ones. This difference must be associated with the different coordination angles at the metal. In the three copper complexes in Table 4 this angle varies by 6.3°, while in the Mn and Re complexes the difference between the two molecules in their unit cells is 6.1 and 4.3°, respectively. Furthermore, variations in the C−S−M angle are directly correlated with variations in θ; large values of θ^m give rise to smaller C−S−M angles. The overall picture therefore is one in which the Tm ligand is held fairly rigidly within the crystal lattice, but the coordinative flexibility of the sulfur donors allows the metal fragment to be relatively free to rotate over a small range of angles (up to ca. 7° in the complexes discussed) determined by interligand steric interactions and/or crystal packing forces, while still being constrained by its membership of the bicyclo[3.3.3] cage structure. It is important to appreciate that the atomic motions of the cage atoms involved in this variation of θ are not those involved in the pathway between the C_3 symmetric ground-state structure and the C_{3v} symmetric transition state in the nondissociative inversion of the cage (Figure 2), as that requires a concerted variation of θ and ω from their ground-state values of ca. 45 and 60° to 0 and 90°, respectively, at the transition state. The observed flexibility of θ in the solid state does not therefore necessarily imply anything about the energy of the cage inversion process in which angle strain at every atom in the cage will play a role, not just those at sulfur which is arguably the most flexible in this respect. This is further discussed in relation to the results of the ab initio calculations below.

Racemization in Four-Coordinate Complexes. The possible mechanisms responsible for inversion of the metal−Tm cage structure in complexes of six-coordinate metals have been discussed in the Introduction (Figure 2). While an essentially similar nondissociative process of inversion may be envisaged for complexes with four-coordinate metals (Figure 6), the dissociative process must be different. The inversion of the three-coordinate metal center following dissociation of one sulfur donor (a process in reality likely to occur via a trigonal-planar metal center) cannot be involved in the process as subsequent re-coordination would not result in the enantiomeric structure, but rather one of C_{3v} symmetry in which the fourth, non-Tm, ligand is encapsulated within the cage structure directed toward the boron atom (Figure 7). A more likely scenario is that upon dissociation the remaining eight-membered ring inverts and

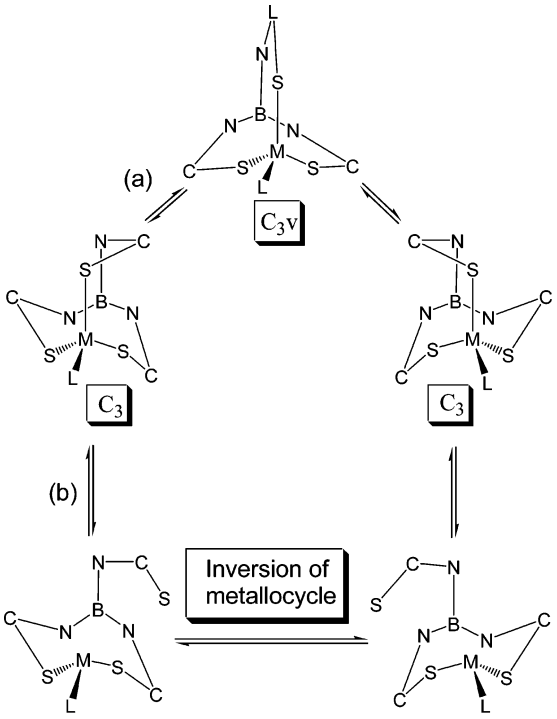

Figure 6. Nondissociative (a) and dissociative (b) mechanisms of racemization for Tm complexes with four-coordinate metals.

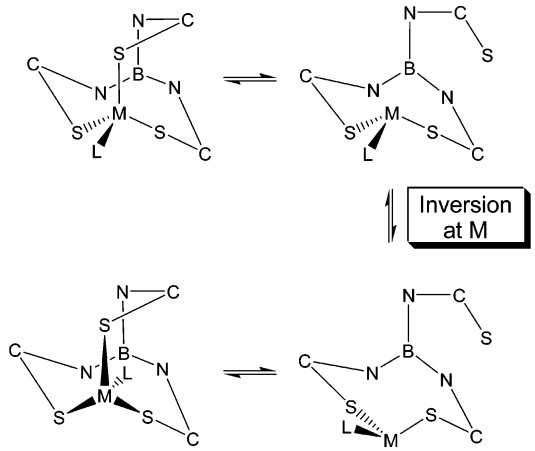

Figure 7. Untenable outcome of inversion at the metal following dissociation of one sulfur donor.

re-coordination of the tripod donor arm provides the enantiomeric system (Figure 6). For the two remaining metal-coordinated donor arms, the motions of the atoms during this process are similar to those occurring during the nondissociative racemization process. However, the overall energy of the process will be lower as the required motion is not hindered by the presence of a bicyclic cage structure which imposes significant angle strain at the C_{3v} symmetric transition state. Analysis of molecular models indicates that this is due to the higher conformational mobility of the metal and/or boron center(s) once one of the ligand tripod arms is dissociated.

The possibility that the alternative Tm coordination mode,[16] in which the ligand binds to the metal through two sulfur atoms and one B−M−H interaction, is present in the complexes reported may be discounted. Not only were the low-frequency B−H signals characteristic of this type of coordination[16] absent from the ^{1}H NMR spectra, but this coordination mode results in a mirror plane in the Tm−metal unit, resulting in an achiral structure. As presented below, it is clear from the NMR spectra obtained for our new complexes that they are chiral and the Tm^{Et} and Tm^{Bn} ligands must therefore be coordinated in the κ^3-S_3 mode, which provides C_3-symmetry.

Variable-Temperature NMR. The chirality of the cage structure in Tm−metal complexes renders the methylene protons of the ethyl and benzyl groups in the Tm^{Et} and Tm^{Bn} ligands diastereotopic and they may therefore be distinguished in ^{1}H NMR spectra of their complexes and represent an AB type spin system. In the case of complexes containing the Tm^{Bn} ligand therefore, a simple 4-line pattern with intensities characteristically distorted by second-order effects, should be observed for the benzyl methylene groups. In the fast-exchange regime the methylene protons become equivalent and a singlet is observed. For Tm^{Et} complexes the situation is complicated by coupling to the adjacent CH_3 group, and this represents an ABX_3 spin system. As will be seen in the experimental spectra, second-order effects in this system result in the appearance of a 12-line pattern of signals. In the fast-exchange limit, the methylene protons are no longer diastereotopic and a single quartet is observed. Where coalescence could be attained within the temperature range accessible to the spectrometer, the activation energy of the racemization process ($\Delta G^{\ddagger}$) may be calculated from the coalescence temperature (T_c) using the equation $\Delta G^{\ddagger} = RT_c[22.96 + \ln(T_c/\Delta\nu)]$, where $\Delta\nu$ is the frequency separation of the signals in the slow-exchange limit.[17]

Four-Coordinate Complexes. The variable-temperature NMR (VT NMR) spectra of [$ZnTm^{Et}Cl$] (**3**) in the methylene region in tetrachloroethane-d_2 are shown in Figure 8c. At 292 K 12 lines are observed in two 6-line signals separated by 65 Hz; the geminal and vicinal couplings are 14.1 and 7.1 Hz, respectively. As the temperature is increased, a certain amount of broadening is observed; however, coalescence is beyond the accessible temperature range. The only conclusion which may be drawn, therefore, is that the coalescence temperature is higher than 373 K and this corresponds to an energy barrier to racemization of >77 kJ mol^{-1}.

The VT NMR spectra of **3** were also recorded from DMSO-d_6 and acetonitrile-d_3 solutions (Figure 8a,b). The highest safely accessible temperature in acetonitrile is 348 K (BP = 354 K), and this is unfortunately slightly below the coalescence temperature. The activation energy in this solvent can therefore only be approximated (>72 kJ mol^{-1}), but it is clear that it is significantly lower than in the non-coordinating tetrachloroethane solvent. In DMSO-d_6 the coalescence temperature is even lower than in acetonitrile and is observed at approximately 293 K. As the temperature is raised further, the fast-exchange limiting spectrum, represented by a quartet, is observed. Slow exchange could not be observed because of the high melting point of DMSO, and a value for $\Delta\nu$ could not therefore be obtained; however, if it is assumed that it has the same value as in acetonitrile solution (50 Hz), the activation energy may be calculated to be 60 kJ mol^{-1}. It is clear that increasing the coordinating ability of the solvent has a significant effect on the energy of the process, and we interpret this as supporting the operation of the dissociative mechanism of racemization (Figure 6) since coordination of the solvent to the metal concomitant with Tm sulfur dissociation will reduce the activation barrier to this first step in the mechanism. This is also evidence for rate determination by this dissociation step in non-coordinating solvents, which is perhaps unsurprising as the subsequent inversion of the eight-membered metallocycle is likely to be a lower energy process than M−S dissociation. In coordinating solvents we are unable to determine from the information available whether solvent coordination precedes or follows dissociation of the Tm sulfur donor arm (i.e. whether the process involves a five- or three-coordinate transition state) and therefore whether solvent coordination or partial Tm dissociation is rate-limiting. Nevertheless it is clear that the process involves a dissociative step.

(16) Foreman, M. R. St. J.; Hill, A. F.; Owen, G. R.; White, A. J. P.; Williams, D. J. *Organometallics* **2003**, *22*, 4446.

(17) Ernst, R. R.; Bodenhausen, G.; Wokaun, A. *Principles of Nuclear Magnetic Spectroscopy in One and Two Dimensions*; Clarenden Press: Oxford, U.K., 1987.

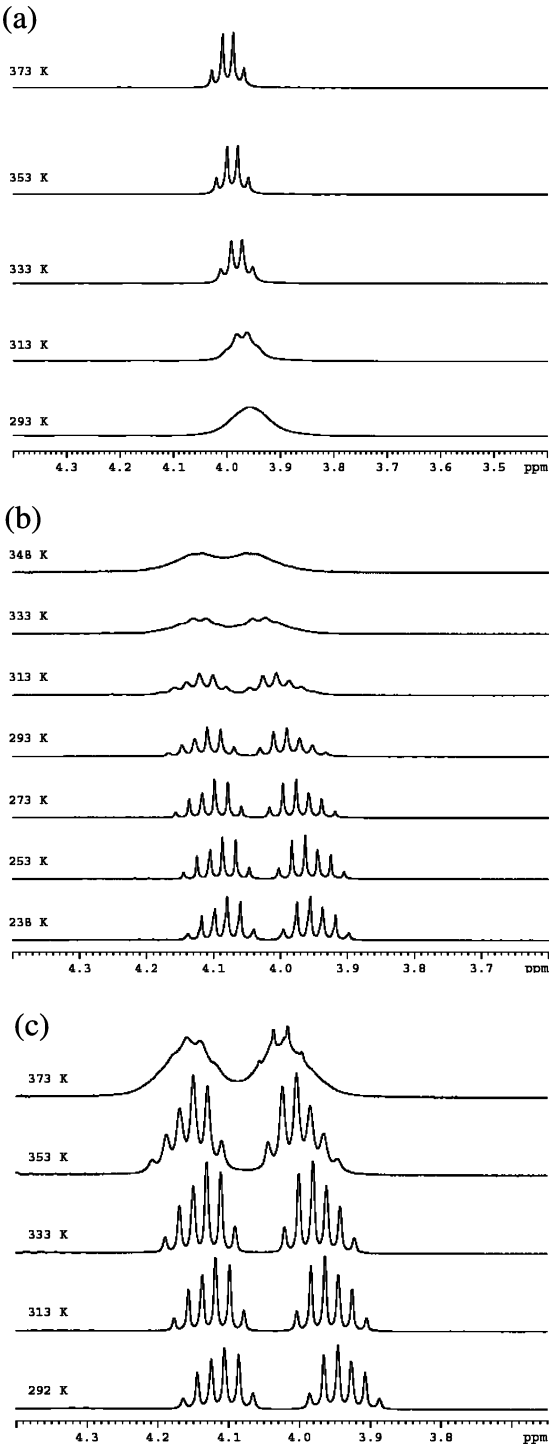

Figure 8. VT NMR spectra of [ZnTm^{Et}Cl] (**3**) in the methylene region in different solvents: (a) DMSO-d_6, (b) acetonitrile-d_3, and (c) tetrachloroethane-d_2.

In tetrachlorethane-d_2 the VT NMR spectra of [ZnTm^{Bn}Cl] (**8**) show the expected slow limit AB type spectrum with a geminal coupling of 15 Hz at 293 K (Figure 9a). Increasing the temperature to 373 K leads to broadening within the doublets but no coalescence between them, and it may be concluded that the activation barrier in this solvent is >77 kJ mol^{-1}. However, in DMSO-d_6 coalescence is observed at approximately 303 K, but slow exchange cannot be observed (Figure 9b). It is therefore necessary to assume that the separation between signals at the slow-exchange limit

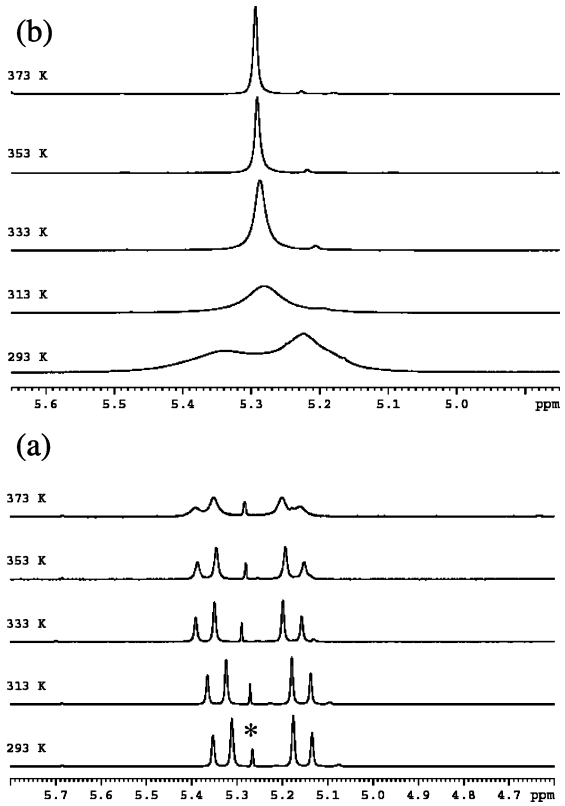

Figure 9. VT NMR spectra of [ZnTm^{Bn}Cl] (**8**) in the methylene region in different solvents: (a) tetrachloroethane-d_2 and (b) DMSO-d_6. The asterisk (*) indicates CH_2Cl_2 impurity.

($\Delta\nu$) is the same as in tetrachlorethane, and this provides an estimated activation energy of 60 kJ mol^{-1}. At higher temperatures the signal resolves into a sharp singlet at the fast-exchange limit. Substitution of *N*-ethyl by *N*-benzyl therefore has little or no effect on the activation energy of the racemization process. This is perhaps not surprising when the crystal structure of [ZnTm^{Bn}Br] is examined.[12] This shows the *N*-benzyl groups to be directed well away from both the bromide ligand and each other and therefore to have minimal steric effect on the structure of the metal−ligand cage structure. This is confirmed by the similarity of the torsion angles (θ^m) in the structures of [ZnTm^{Et}Cl] and [ZnTm^{Bn}Br], which are 46.3 and −46.5°, respectively, the difference in sign simply reflecting $\lambda\lambda\lambda$ and $\delta\delta\delta$ stereochemistry of the complexes, respectively.[3]

Cadmium complex **4** was subjected to VT NMR experiments in tetrachloroethane-d_2, and the spectra obtained are presented in the Supporting Information. At room temperature a 12-line signal is observed for the methylene protons, similar to that observed for the Zn complex **3** (Figure 8c) and consistent with slow exchange. The geminal and vicinal couplings are 14.1and 7.1 Hz, respectively, and $\Delta\nu$ between the 6-line signals is 54 Hz. Coalescence is found to occur at approximately 373 K, and the energy barrier to racemization of the complex is therefore 77 kJ mol^{-1}, a lower value than that for its zinc analogue **3** in the same solvent for which coalescence occurs above 373 K. The coalescence temperature for complex **4** in acetonitrile-d_3 is observed at 333 K and the energy barrier to racemization is therefore 69 kJ mol^{-1}. This lower value in a coordinating solvent again

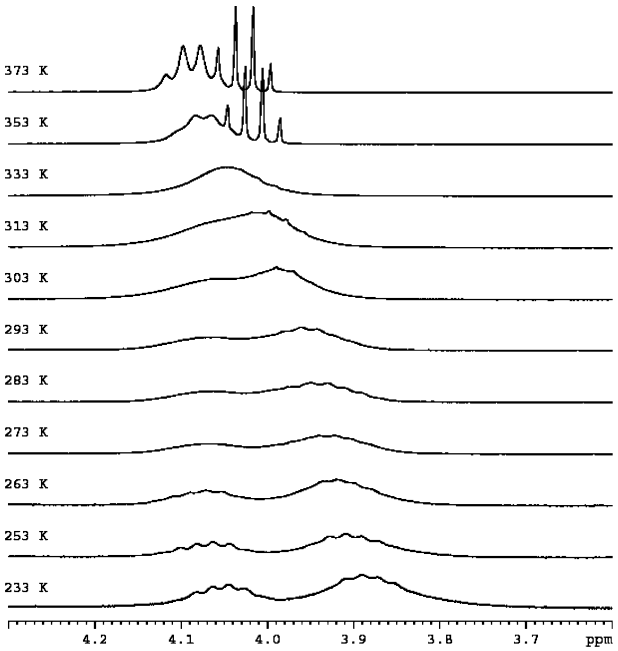

Figure 10. VT NMR spectra of [HgTm^{Et}Cl] (**5**) in tetrachloroethane-d_2 solution.

strongly implicates the operation of the dissociative mechanism (Figure 6). The lower activation energy for the Cd complex compared with that for the Zn one is also consistent with this conclusion given the anticipated greater lability of the larger metal ion. As with the zinc complex (**3**), the results from VT NMR experiments with **4** in DMSO-d_6 do not reveal much information about the slow-exchange processes, but it is clear that the more strongly coordinating solvent lowers the activation energy still further. At 293 K, the lowest accessible temperature in this solvent, a broad signal with weakly discernible quartet structure is observed. This indicates that the coalescence point is somewhat below this temperature. Although slow exchange is not observed, if the value of $\Delta\nu$ obtained in tetrachloroethane (58 Hz) is used, an energy barrier for the racemization of the complex of $<$60 kJ mol^{-1} is obtained.

In the VT NMR spectra of [HgTm^{Et}Cl] (**5**) in tetrachloroethane-d_2 a low-temperature limiting spectrum could not be observed at the lowest accessible temperature (233 K) (Figure 10). Coalescence of the two broad signals is observed at approximately 333 K. As the temperature is increased further, the signals begin to sharpen into a quartet, but in addition a further sharp quartet appears in the spectra between 333 and 353 K. The reversibility of this transformation in the spectra was confirmed by recooling the sample, which regenerated the earlier low-temperature spectra. The sharp quartet cannot therefore be due to irreversible high-temperature decomposition of the complex. A further anomaly in these spectra is the integration ratio of the two signals observed at low temperature, which is 2:1 and not 1:1 as required for the diastereotopic protons in a four-coordinate complex, as seen for the Zn and Cd complexes above. Furthermore, two methyl signals in a similar ratio are observed in the spectra at these low temperatures.

Scheme 1. Disproportionation of [HgTm^{Et}Cl] (**5**) To Give [Hg(Tm^{Et})$_2$] Which May Explain the High-Temperature NMR Spectra of **5**

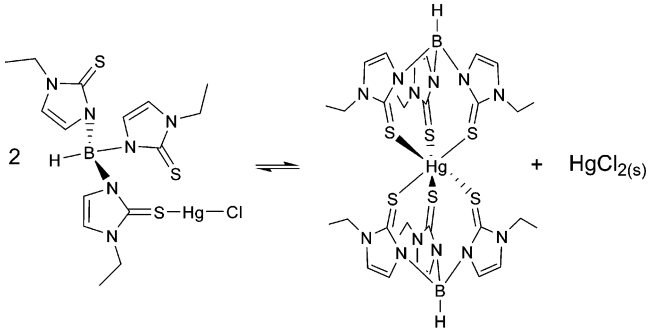

We therefore conclude that the Tm^{Et} ligand is not coordinated as a κ^3 tripod in this complex, but rather the mercury is present in a linear two-coordinate environment. This would provide the 2:1 ratio observed for both the methylene and methyl signals due to the uncoordinated and coordinated arms of the ligand. The signals are broad even at low temperature because the metal is exchanging between sulfur sites on the ligand, and at approximately 333 K coalescence is observed due to this process. The activation energy of this process may be estimated to be 68 kJ mol^{-1} using a value of 65 Hz for $\Delta\nu$ approximated from the incompletely sharpened signals observed at 233 K. This explanation, however, does not account for the origin of the sharp quartet which appears in the spectrum at 353 K. Although the signal is absent in the room-temperature spectrum recorded after the high-temperature VT NMR experiments were carried out, this does not rule out reversible partial dissociation of the Tm^{Et} ligand at high temperature giving rise to this signal. However, an alternative explanation involves reversible formation of the complex [Hg(Tm^{Et})$_2$], containing an octahedrally coordinated mercury center, via disproportionation of the two-coordinate [HgTm^{Et}Cl] complex (Scheme 1). Although the ligands are coordinated κ^3 in this complex, the presence of an inversion center results in an achiral complex and the methylene protons would be observed as a simple sharp quartet.

In acetonitrile-d_3 a similar pattern of signals is seen as the temperature changes whereby, at low temperature, two broad signals with an unequal integration ratio are observed and as the temperature is increased, coalescence followed by fast exchange providing a single quartet is observed. The additional sharp quartet is absent from the high-temperature spectra recorded in this solvent. The coalescence temperature of approximately 273 K provides an activation energy for site exchange of 57 kJ mol^{-1}. It is not clear why a change to a more coordinating solvent should reduce the activation energy for this site exchange process at the two-coordinate Hg ion unless the process is dissociative involving a [Hg(solvent)Cl]$^+$ intermediate species. However, this seems an unlikely process to be promoted by a nitrogen donor solvent at mercury(II) in competition with a sulfur donor, although it would be entropically neutral and driven by the excess of the acetonitrile present. Unfortunately, spectra recorded in DMSO-d^6 do not provide any further clues to the reason for this as the lowest accessible temperature (293

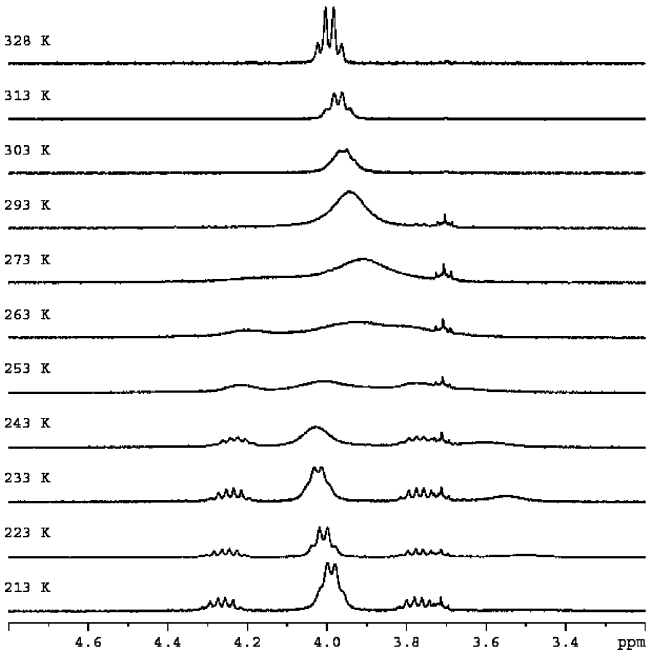

Figure 11. VT NMR spectra of [AgTm^{Et}(PPh$_3$)] (**7**) in the methylene region in chloroform-*d* solution.

K) is somewhere way beyond coalescence and an energy cannot therefore be calculated. VT NMR spectra of [HgTm^{Bn}Cl] are also unhelpful as a singlet representing fast exchange is observed at all temperatures, only broadening significantly, although not reaching the coalescence point, in tetrachloroethane at 213 K.

In the VT NMR spectra of **6** in chloroform-*d* a pair of sharp 6-line signals is observed at 213 K for the methylene protons, indicating slow interconversion between enantiomers. The geminal and vicinal couplings are 13.9 and 7.0 Hz, respectively, and $\Delta\nu = 119$ Hz. Coalescence of these signals occurs at approximately 278 K. As the sample is heated further, the signals sharpen and a quartet, characteristic of fast exchange, is observed. The energy barrier for the racemization of the complex is therefore approximately 55 kJ mol^{-1}. This value is somewhat lower than the energies found for group 12 complexes. If we assume that the dissociative mechanism is operating, this is consistent with the lower M−S dissociation energy expected for this d^{10} unipositive metal ion. Changing the solvent to acetonitrile-d_3 has a somewhat smaller effect on the activation energy of the process compared with that observed for the Zn and Cd complexes. Coalescence is observed at 263 K, giving a value of 54 kJ mol^{-1} for the energy barrier to racemization. Spectra were not recorded in DMSO.

The VT NMR spectra of [AgTm^{Et}(PPh$_3$)] (**7**) in chloroform-*d* are shown in Figure 11. Initially the room-temperature (293 K) spectrum was recorded and a broad signal was observed, which was assumed to be the coalescence of the signals for the diastereotopic protons; however, when the low-temperature spectra were recorded, an unexpected pattern emerged. In the slow-exchange region two separate sets of signals are observed, one of which is similar to the expected pattern for the diastereotopic methylene protons and the other appears to be a broad quartet. Additional signals

Scheme 2. Equilibrium between Three- and Four-Coordinate Ag in [AgTm^{Et}(PPh$_3$)] (**7**)

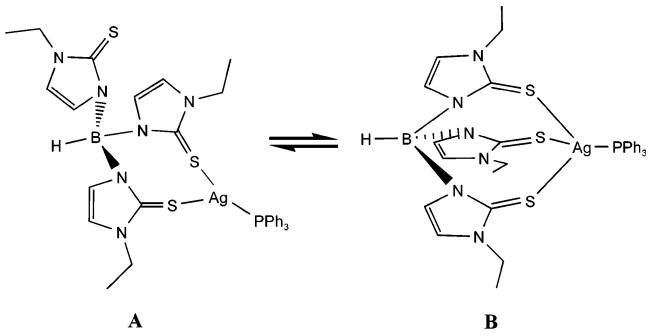

are also observed in the methyl and imidazole (CH) regions of the spectra. It appears therefore that there are two species present, giving rise to two sets of signals which broaden as the temperature is raised. The PCy$_3$ analogue of **7** containing the parent Tm ligand, [AgTm(PCy$_3$)], has been structurally characterized and found to contain a three-coordinate silver ion with the Tm ligand κ^2-coordinated,[18] and a similar coordination mode has been suggested to account for the NMR spectroscopic properties of its triphenylphosphine analogue [AgTm(PPh$_3$)].[19] We therefore propose that both three- and four-coordinate Ag complexes are present in solution in which the Tm^{Et} ligand is bi- and tridentate, respectively (Scheme 2). Furthermore, the spectra suggest that in the three-coordinate species (**A**) the silver is undergoing rapid site exchange between sulfur donors, thereby equilibrating the heterocycle groups which therefore display triplet and quartet signals for the methyl and methylene protons, respectively. The imidazole protons appear as a doublet and do not give any further insight into the geometry. At low temperature the four-coordinate species (**B**) displays, as expected, a 6-line signal for each of the diastereotopic methylene protons and a triplet for the methyl protons. These signals are observed to coalesce as the temperature is increased. At 213 K the geminal and vicinal couplings are 13.9 and 7.0 Hz, respectively. The integration of the signals confirms the relationship between the quartet at 3.99 ppm and the triplet at 1.26 ppm for **A**, and between the multiplets at 3.77 and 4.26 ppm and the triplet at 1.14 ppm for **B**. The coalescence due to the metal−ligand cage inversion process for the four-coordinate species (**B**) occurs at approximately 273 K; this along with a $\Delta\nu$ value of 188 Hz provides an activation energy of approximately 53 kJ mol^{-1}. This is only slightly lower than the activation energy found for its copper analogue (**6**). The fact that a single quartet is observed at high temperature indicates an equilibration of the three- and four-coordinate species, providing a coalescence of the low-temperature quartet and 12-line signals, which appears to occur at approximately the same temperature as that due to the cage inversion process (273 K). The results from the VT NMR of **7** in acetonitrile do not provide any further insight into the processes as slow exchange is below the lowest

(18) Santini, C.; Pettinari, C.; Gioia Lobbia, G.; Spagna, R.; Pellei, M.; Vallorani, F. *Inorg. Chim. Acta* **1999**, *285*, 81.
(19) Santini, C.; Gioia Lobbia, G.; Pettinari, C.; Pellei, M.; Valle, G.; Calogero, S. *Inorg. Chem.* **1998**, *37*, 890.

accessible temperature for this solvent. However, coalescence occurs at approximately this temperature (238 K), and the energy barrier for the inversion may therefore be estimated to be approximately 46 kJ mol^{-1}. Spectra were not recorded from DMSO solution.

Six-Coordinate Complexes. The VT NMR spectra of $[MnTm^{Et}(CO)_3]$ (**11**) in tetrachloroethane-d_2 are weak due to the very low solubility of the complex; however, a pair of 6-line signals can be seen which remain unchanged from 293 K up to the highest accessible temperature (373 K). The geminal and vicinal couplings are 14.0 and 7.0 Hz, respectively. Since neither coalescence nor, indeed any change at all is observed with increasing temperature, nothing can be said about the operation of a mechanism of racemization. However, it is obvious that if this is occurring, its activation energy is very much higher than that observed in the four-coordinate complexes studied. The spectra were also recorded from DMSO-d_6 solution, but again no broadening was observed up to 373 K. The low-spin d^6 electronic configuration of the Mn(I) in this complex makes it substitutionally inert. The dissociation of one of the sulfur donors of the Tm^{Et} ligand is therefore a high-energy process, and the presence of DMSO has no effect on the spectra. Given the low energy of the Berry pseudorotation process, if dissociation were occurring on the NMR time scale, racemization would be observed. Notwithstanding that the activation energies of the dissociative mechanism of racemization will differ because of the different angles at the metal, the absence of any observed racemization process on the NMR time scale in this inert Mn(I) system provides additional support for the conclusion that inversion in the labile four-coordinate systems occurs via a dissociative mechanism.

The complexes $[RuTm^{Et}(p\text{-cymene})]X$ [X = Cl (**9**), PF_6 (**10**)] gave somewhat unexpected results when NMR spectra were recorded in a range of solvents. In tetrachloroethane-d_2 and DMSO-d_6 an apparent quartet is observed for the methylene protons of **9** (Figure 12a). This appears to suggest that either the complex is racemizing very rapidly on the NMR time scale or that the complex is achiral in solution, despite its chiral solid-state structure discussed above. Neither of these interpretations is consistent with the inert low-spin d^6 electronic configuration, which, for Mn(I), was shown to provide a very high barrier to racemization. The first clue that the appearance of the methylene signals must be due to accidental coincidence of the signals from the diatereotopic protons came from the appearance of the *p*-cymene arene CH signals. These usually appear as a clear $(AB)_2$ system (Figure 13a);[14,15] however, in all of the spectra of **9** and **10** recorded in this work these protons appear as four doublets (Figure 13b), one representing each inequivalent proton, thus indicating their diastereotopic nature and confirming that the C_3-symmetric chiral Tm^{Et}–Ru structure is retained in solution. The *p*-cymene isopropyl methyl groups are also revealed to be diastereotopic in this complex, providing two signals in both the ^1H and ^{13}C NMR spectra, separated by 0.01 and 0.58 ppm, respectively.

The spectra of **9** in chloroform-*d* and acetonitrile-d_3 reveal the hidden complexity of the methylene proton signals and

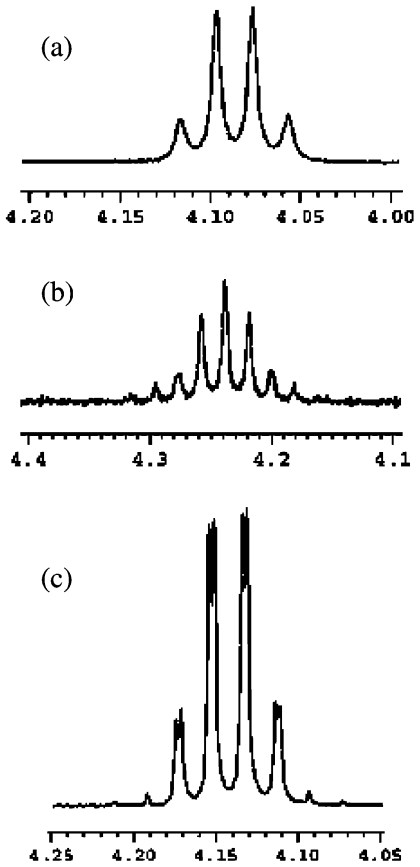

Figure 12. ^1H NMR spectra of $[RuTm^{Et}(p\text{-cymene})]Cl$ (**9**) at 293 K in different solvents: (a) tetrachloroethane-d_2, (b) chloroform-*d*, and (c) acetonitrile-d_3.

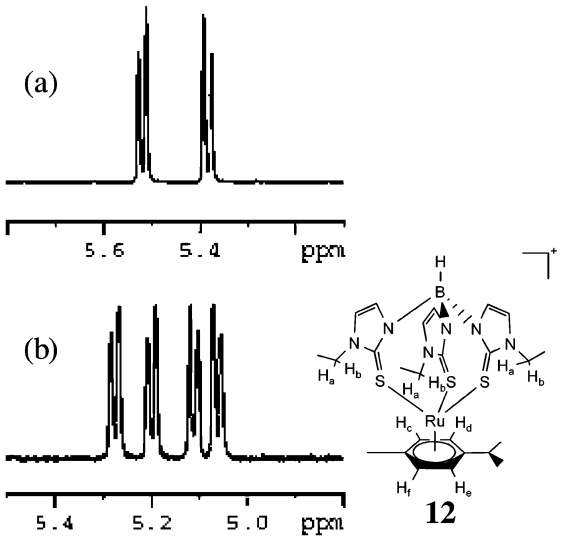

Figure 13. ^1H NMR spectra of the arene CH protons in the Ru(*p*-cymene) fragment in (a) $[Ru(p\text{-cymene})Cl_2]_2$ and (b) $[RuTm^{Et}(p\text{-cymene})]Cl$ (**9**).

confirm the conclusion drawn from the arene CH signals. In acetonitrile-d_3 the two multiplets due to the diasteriotopic protons are separated by just 1.8 Hz, while in chloroform-*d* this is increased to 7.2 Hz (Figure 12). This solvent effect on the spectra is especially surprising given the similarity of chloroform-*d* and tetrachloroethane-d_2; however, the result is reproduced when the chloride counterion is exchanged for

PF_6^- and the spectra of **10** in chloroform-*d* and tetrachloroethane-d_2 display a similar set of signals. The spectra of these Ru complexes are invariant up to 373 K, the highest temperature recorded. It is clear that the separation between signals for the diastereotopic protons in **9** and **10** is very small, and in tetrachloroethane-d_2 and DMSO-d_6 solutions the line width is such that the two signals cannot be resolved. As the value of $\Delta\nu$ approaches zero (i.e. the signals for the diastereotopic protons coincide), the calculated value for the activation energy of the inversion process becomes significantly larger than for any other complex studied. At 373 K, a value of $\Delta\nu = 1$ Hz gives an activation energy of >90 kJ mol^{-1}, however, in reality the activation energy is a good deal higher than this as even spectra recorded at 373 K show no signs of broadening and the coalescence temperature will therefore be substantially higher than this. An activation energy of 150 kJ mol^{-1} would give rise to a coalescence temperature of 615 K for example. This gives a good indication that, as previously mentioned, the energy barrier to racemization in six-coordinate complexes with inert metal centers is considerably higher than for four-coordinate complexes and that the energy barrier to the nondissociative *twist* mechanism of racemization is high.

Ab Initio Calculations. Ab initio molecular orbital (MO) geometry optimizations (MP2 method, LanL2DZ basis set) were carried out on model four-coordinate zinc(II)-centered and six-coordinate manganese(I)-centered C_3-symmetric complexes. Both the ground-state structures and the transition-state structures in the nondissociative inversion mechanism (Figures 2a and 6a) were optimized. From the differences between the calculated absolute energies of these structures activation energies were established for the nondissociative "twist" mechanism occurring in the isolated complexes. The calculated structures are shown in Figure 14.

For zinc the system $[HB(C_3H_3N_2S)_3ZnCl]$ was employed as a simplified structure analogous to [ZnTmCl]. We can be confident that this simplification should not have a substantial affect on the steric contribution to the calculated energy as the replacement of the *N*-alkyl group with N−H should not substantially affect the angle strain generated in the C_{3v} symmetric transition state because all of the strained atoms have been retained in the model structure. The calculated energy difference between the ground- and transition-state structures for this system is 121 kJ mol^{-1}. This value is substantially higher than that obtained experimentally for $[ZnTm^{Et}Cl]$ (**3**) and $[ZnTm^{Bn}Cl]$ (**8**) (approximately 60 kJ mol^{-1} in DMSO-d_6 solution). The conclusion from the VT NMR results that four-coordinate zinc complexes undergo dissociative racemization is therefore supported by comparison of calculated and experimental results. For the calculations on the manganese complex the model system $[HB(C_3H_3N_2S)_3Mn(CO)_3]$ was employed. The calculated energy difference between the ground- and transition-state structures is 163 kJ mol^{-1}. Using our VT NMR technique, we have been unable to observe any sign of dynamic behavior in complexes of six-coordinate metals, in either coordinating or noncoordinating solvents; this is not surprising in view of the fact that coalescence of signals in our system due to a process with an activation energy of 163 kJ mol^{-1} would not be observed below 700 K. A dissociative mechanism of racemization may have a lower activation barrier than this; however, the question of whether racemization occurs via the dissociative or nondissociative mechanism (Figure 2) in these complexes with substitution-inert six-coordinate metals is a moot point as we currently have no evidence for either.

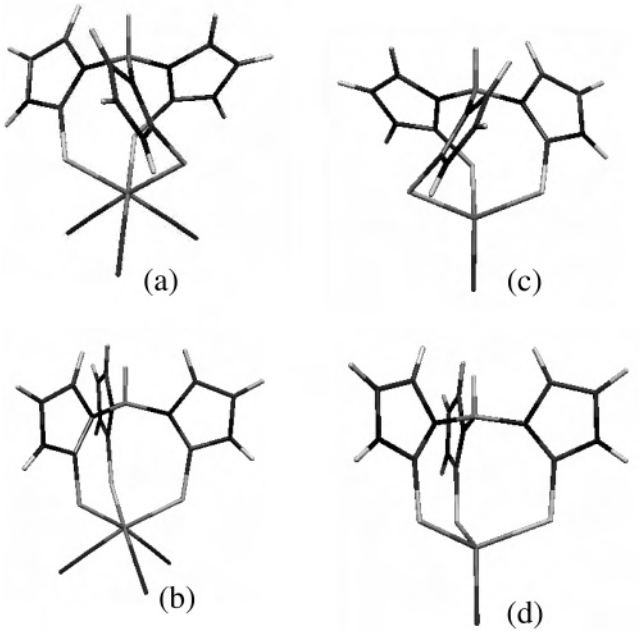

Figure 14. Ground-state (C_3) and transition-state (C_{3v}) structures for $[HB(C_3H_3N_2S)_3Mn(CO)_3]$ (a and b) and $[HB(C_3H_3N_2S)_3ZnCl]$ (c and d) resulting from ab initio DFT calculations. See Table 5 for metrical data.

Table 5. Angles within the Bicyclo[3.3.3] Tm−M Cage Obtained from ab Initio Calculations on the Model Complexes $[HB(C_3H_3N_2S)_3ZnCl]$ and $[HB(C_3H_3N_2S)_3Mn(CO)_3]$

	$[HB(C_3H_3N_2S)_3ZnCl]$		$[HB(C_3H_3N_2S)_3Mn(CO)_3]$	
	ground state	transition state	ground state	transition state
S−M−S	102.0	109.9	93.9	99.3
C−S−M	96.3	113.7	103.5	125.8
N−C−S	131.9	137.1	131.2	138.3
B−N−C	131.1	138.4	129.3	135.8
N−B−N	111.7	116.9	110.9	113.3

The calculated activation energy for nondissociative racemization of the model four-coordinate zinc(II) complex is significantly lower than that for the six-coordinate manganese(I) complex. We interpret this as being due to differences in angle strain for the two different metals induced by the *untwisting* of the structures. The ab initio calculations indicate that as the path between the ground and transition states is traversed, the S−M−S angles are increased by 7.9° (Table 5) in the zinc structure and by 5.4° in the manganese one. The zinc center attains an almost ideal tetrahedral angle in the transition state, and even if this were not the case, Zn(II) does not impose any preferred coordination geometry and significant angle strain at the metal is therefore unlikely. With this in mind, and disregarding the effects of metal size, it could be argued that the angle of ca. 110° observed in the transition-state Zn structure is the optimum for a metal−Tm complex at its transition state,

Table 6. Experimental and Calculated Activation Energies for Racemization of Tm^{Et} andTm^{Bn} Complexes

	activation energy/(kJ mol^{-1})			ab initio calcd activation energy/(kJ mol^{-1})[e]
	in noncoordinating solvent	in acetonitrile-d_3	in DMSO-d_6	
[$ZnTm^{Et}Cl$] (**3**)	>77[a]	>72	60	121
[$CdTm^{Et}Br$] (**4**)	77[a]	69	<61	
[$HgTm^{Et}Cl$] (**5**)	68[a,b]	57[b]		
[$CuTm^{Et}PPh_3$] (**6**)	55[c]	54		
[$AgTm^{Et}PPh_3$] (**7**)	53[c]	45−50		
[$ZnTm^{Bn}Cl$] (**8**)	>77[a]		60	
[$RuTm^{Et}$(*p*-cymene)]$^+$ (**9**)	≫79[c,d]			
[$MnTm^{Et}(CO)_3$] (**11**)	≫77[a,d]		≫78[d]	163

[a] Tetrachloroethane-d_2. [b] Energy for sulfur site exchange in a linear two-coordinate complex. [c] Chloroform-*d*, n/a (not applicable). [d] Energy derived from spectra recorded at the highest accessible temperature in each solvent. [e] Calculated for nondissociative racemization of N−H containing analogues.

regardless of the coordination number of the metal. The low-spin d^6 configuration of Mn(I) provides a strong preference for angles of 90°, and with S−M−S angles of 99.3° the strain at the metal center will therefore be considerably higher in this six-coordinate complex at the transition state. This is supported by the smaller change in angle between ground and transition states than in the Zn complex and the 10° discrepancy from the notional ideal of 110°. This relative geometric rigidity of the Mn(I) center results in somewhat larger changes in angle between ground and transition states occurring elsewhere in the structure compared to those found in the zinc complex. The C−S−M angles increase by 17.4 and 22.3° in the Zn and Mn complexes, respectively, and it therefore appears that instead of substantially altering the angles at the metal, it is the angles at sulfur that are distorted in the manganese complex at the transition state. The large changes in the angles at sulfur indicate its geometric flexibility as previously noted in the discussion of the solid-state structures of metal Tm complexes. One route to complexes with increased barriers to nondissociative racemization would therefore appear to be to replace the sulfur atoms with geometrically less flexible donors, a goal which we are currently exploring. There are only relatively minor discrepancies between changes in the remaining corresponding angles within the cages for the Zn and Mn complexes. The overall picture, therefore, is one in which the geometric rigidity of the metal center in the Mn complex increases the energy to the transition state by more than that found in the complex of the geometrically flexible Zn(II), and this is reflected in increases in angle strain elsewhere in the Mn−Tm cage structure.

Conclusions

The experimental activation energy data for racemization of Tm^{Et} and Tm^{Bn} complexes are presented in Table 6 along with the energies derived from the ab initio calculations. The use of the Tm^{Et} and Tm^{Bn} ligands has proved to be a powerful tool in revealing the details of the solution behavior of their complexes with four-coordinate metal ions. It is clear from the effects of donor solvents on the activation energies that the racemization occurs via the dissociative mechanism (Figure 6). The energy term associated with the coordination of a donor to the metal concomitant with dissociation of one of the Tm ligand sulfur donors reduces the energy of this rate-determining step and therefore the activation energy of the racemization process substantially (Figure 15). The process appears to follow the dissociative mechanism even in the absence of an external donor. This is strongly implicated by the large difference between the activation energy for the racemization of **3** in tetrachloroethane-d_2 which, although full coalescence could not be observed at 373 K, is clearly only marginally above 77 kJ mol^{-1} (Figure 8c) and the value of 121 kJ mol^{-1} calculated for the activation energy for the nondissociative mechanism for its N−H containing analogue. Given the d^{10} electronic configuration of the metal ions studied, the low energy of this process is easily understood on the basis of their high substitution lability. Furthermore, for the complexes containing d^{10} metal ions the comparison between the activation energies measured for the group 12 metal(II) complexes **3** and **4** and the group 11 metal(I) complexes **6** and **7** show an inverse correlation with metal size consistent with a dissociative process in which electrostatic factors play a significant role.

The activation energy for racemization of the six-coordinate complexes of Mn(I) and Ru(II) lay above the range accessible to the VT NMR line shape analysis method, and no evidence for racemization could be obtained for these complexes. The ab initio calculations provide an indication of the size of the energy barrier to racemization if the process is nondissociative. If this is indeed the case, the process may accurately be described as racemization by atropisomer interconversion. An activation energy of 163 kJ mol^{-1} for this process indicates that the half-life for interconversion should be sufficiently long to allow resolution of the atropisomers, which will facilitate a full kinetic analysis of the interconversion process, and we are currently investigating this possibility. Kinetic and thermodynamic data that may be used to support a discussion of the likely dissociation

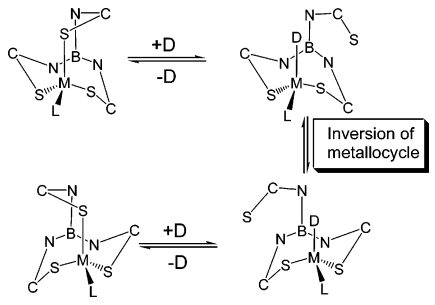

Figure 15. Donor-assisted dissociative racemization of Tm complexes with four-coordinate metal ions.

energy of one of the sulfur donors of a Tm ligand from a kinetically inert metal ion are sparse. For acetonitrile coordinated to Ru(II) a revealing study has shown that the rate of exchange in $[Ru(NCMe)_6]^{2+}$ is very slow ($\log k = -11$, $\Delta G^{\ddagger} = 130$ kJ mol^{-1}) but that in the heteroleptic complex $[Ru(\eta\text{-}C_6H_6)(NCMe)_3]^{2+}$ the presence of the arene ligand has a very substantial effect, reducing $\log k$ to -5 and $\Delta G^{\ddagger}$ to 98 kJ mol^{-1}.[20] Given the presence of an arene ligand in our ruthenium complex **9**, and similarly translabilizing CO ligands in the manganese one **11**, these values suggest that the process of racemization may be dissociative, given the high activation energy calculated for the nondissociative mechanism. The full picture will need to await further investigations of these and related systems.

(20) Luginbühl, W.; Zbinden, P.; Pittet, P. P.; Armbruster, T.; Bürgi, H.-B.; Merbach, A. E.; Ludi, A. *Inorg. Chem.* **1991**, *30*, 2350.

Acknowledgment. We acknowledge the financial support provided through the European Community's Human Potential Program under Contract HPRN-CT-2001-00187 (AC3S).

Supporting Information Available: Full crystallographic details for $[Tm^{Et}ZnCl]$ (**3**), $[Tm^{Et}CdBr]$ (**4**), $[Tm^{Et}Cu(PPh_3)]$ (**6**), and $[Tm^{Et}Ru(p\text{-cymene})]Cl\cdot H_2O$ (**9**), Gaussian 98 output files for calculations conducted on ground- and transition-state structures of the model complexes $[\kappa^3\text{-}HB(C_3H_3N_2S)_3Mn(CO)_3]$ and $[\kappa^3\text{-}HB(C_3H_3N_2S)_3ZnCl]$, VT NMR spectra for $[CdTm^{Et}Br]$ (**4**) in tetrachloroethane-d_2, acetonitrile-d_3, and DMSO-d_6, and $^{13}C\{^1H\}$ NMR spectra for new compounds for which satisfactory elemental analyses could not be obtained (pdf). This material is available free of charge via the Internet at http://pubs.acs.org.

IC0505293